

¹⁶H. Ikegami and G. T. Emery, Phys. Rev. Letters 13, 26 (1964).

¹⁷L. V. Groshev, A. M. Demidov, and N. Shadiev, Izv. Akad. Nauk SSSR, Ser. Fiz. 30, 1136 (1966) [transl.:

Bull. Acad. Sci. USSR, Phys. Ser. 30, 1187 (1967)].

¹⁸S. E. Arnell, R. Hardell, A. Hasselgren, G.-G. Mattsson, and Ö. Skeppstedt, Phys. Scripta 4, 89 (1971).

PHYSICAL REVIEW C

VOLUME 6, NUMBER 5

NOVEMBER 1972

Nuclear Charge Distributions of Isotone Pairs. I. ³¹P and ³²S[†]*

B. B. P. Sinha[‡] and G. A. Peterson

Department of Physics, University of Massachusetts, Amherst, Massachusetts 01002

and

G. C. Li and R. R. Whitney[§]

High Energy Physics Laboratory, Stanford University, Stanford, California 94305

(Received 12 June 1972)

Elastic cross sections for electron scattering from ³¹P and ³²S are given for the momentum-transfer range from 0.7 to 2.9 fm⁻¹. The data were analyzed by means of a phase-shift code using phenomenological Fermi charge distributions modified with small undulations. The difference of the ³¹P and ³²S charge distributions has been compared with a 2s_{1/2} proton distribution and with other nuclear models.

I. INTRODUCTION

High-momentum-transfer elastic electron scattering has provided detailed information about the radial distribution of charge in nuclei. The sensitivity of such measurements has been sufficient to determine differences in charge distributions of nuclei having the same number of protons but varying numbers of neutrons. For example, studies of the calcium isotopes with 250- and 500-MeV electrons by Frosch *et al.*¹ showed that an increase in the charge radius due to the presence of more neutrons in the nuclear volume was counterbalanced by a decrease of the surface thickness as the *f*_{7/2} neutron shell was filled. They used a phenomenological three-parameter static charge distribution to fit the measured cross sections. Higher-momentum-transfer experiments on ⁴⁰Ca and ⁴⁸Ca using 750-MeV electrons by Bellicard *et al.*² showed that additional charge-distribution parameters were required in order to fit the cross sections over the entire momentum-transfer range.

We have started a study of elastic electron scattering from isotones in order to learn how charge distributions change when the number of neutrons is held fixed and the number of protons is varied. A comparison of the charge distributions of two isotones differing by one proton gives an indication of that proton's shell-model-orbit radial charge distribution modified by possible complications due to Coulomb repulsion, pairing, shell closure, and rearrangement effects due to

changes in the nuclear field.

The study of odd-*A* isotones is somewhat more complicated than even-*A* isotones or isotopes because of scattering from multipole moments other than the usual charge monopole, and because such odd-*A* nuclei frequently have low-lying excited states which must be resolved from the ground state.

Here the isotone pair ³¹P and ³²S is considered. These nuclei differ by a 2s_{1/2} proton according to the shell model. A correction for magnetic dipole elastic scattering is necessary for ³¹P, since its ground state spin of $\frac{1}{2}\hbar$ allows both Coulomb monopole and magnetic dipole scattering. In the last section we compare our extracted charge distributions with model calculations.

A forthcoming paper³ will describe a similar comparison between the isotone pair ³⁹K and ⁴⁰Ca, where both nuclei have closed neutron shells, ⁴⁰Ca has a closed proton shell, but ³⁹K lacks one 1d_{3/2} proton from having both shells closed. A preliminary report of the ³⁹K and ⁴⁰Ca comparison has been given.⁴

II. EXPERIMENTAL FEATURES

The experiment was performed at Stanford University by using the Mark III linear accelerator, the 72-in. radius of curvature double-focusing magnetic spectrometer, and other associated apparatus. The details of the experimental equipment and procedures have been reported before¹

and we forego giving many of them here. Beam energies of 250 and 400 MeV were used.

The ^{31}P target was a pressed powder disk of thickness 404 mg/cm². ^{31}P is naturally 100% isotopically abundant. The S target was 418 mg/cm² and of natural isotopic composition. The 4.22% of ^{34}S and 0.76% of ^{33}S were estimated to have negligible effects on the extracted ^{32}S cross sections. Both targets were rotated in the beam in order to distribute heat over the surface of the targets. Also a few torr of hydrogen gas was put into the scattering chamber to aid in heat removal. This gas did not contribute a background because of its large recoil energy loss. For all runs, high enough resolution was used to allow elastic scattering to be separated from the inelastic scattering from the first excited states of ^{31}P at 1.27 MeV and of ^{32}S at 2.24 MeV.

The output of a 100-channel-spectrometer-focal-plane-detector array⁵ was stored in the memory of an IBM-7700 computer.⁶ Calculations of dead-time losses, counter efficiencies, and radiative corrections were made on line, so that cross sections could be obtained directly with all major corrections included.

Because of multiple scattering in the targets, not all of the beam was collected by a Faraday cup located several meters downstream of the targets. Since the target angle and hence the effective target thickness was different for each scattering angle, it was necessary to make small corrections of at most a few percent for the varying beam losses. This was done by comparing the integrated current from a secondary-emission monitor, located upstream of the target, to that of the Faraday cup for a large range of target angles.

Several calibrations made since the work of Frosch *et al.*¹ led to improved accuracy in the cross sections. For this experiment the incident energies were known to $\pm 0.1\%$, the central scattering angle to $\pm 0.03^\circ$, and the incoming beam direction to $\pm 0.02^\circ$. The experimental cross sections were averaged over the spectrometer acceptance angle of $\pm 0.93^\circ$ and are given in Tables I and II as a function of the central scattering angle for center-of-target energies of 250.0 and 400.0 MeV, corresponding to a momentum-transfer range from about 0.7 to 2.9 fm⁻¹. A 3% systematic error was added in quadrature to all data.

III. HIGHER MULTIPOLE CORRECTIONS

The phase-shift code^{7,8} used in this study calculates the scattering only from a charge monopole, $E0$, and does not calculate the scattering from magnetic dipole, $M1$, and other higher multipole

moments. Calculations of the $E0$ scattering from spinless ^{32}S may be made directly with this code without corrections, because no higher multipoles contribute to the scattering. However, in the case of ^{31}P , with spin $\frac{1}{2}\hbar$, the small $M1$ scattering contributions had to be estimated and then subtracted from the experimental cross sections in order to obtain the dominant $E0$ cross section.

A first-Born-approximation single-particle shell-model calculation^{8,9} of these $M1$ contributions was made. It was assumed that the $M1$ moment was due only to the unpaired $2s_{1/2}$ proton in ^{31}P . The calculated results were corrected for Coulomb distortion by scaling them to experimental estimates of higher multipole contributions obtained by making a crude separation of longitudinal (charge) and transverse (current and magnetic) contributions,¹⁰ i.e., by plotting the square of the experimental form factor, F^2 , against $(\frac{1}{2} + \tan^2 \frac{1}{2}\theta)$ for a constant q^2 . Also a comparison of the distorted-wave Born approximation (DWBA) to plane-wave (BA) form factors in general suggested a shift in BA zeros to smaller q^2 corresponding to a DWBA minimum. Thus the BA curve of ^{31}P was compressed until at the same θ and q^2 the calculated results agreed closely with the experimental estimates. In this way it was possible to estimate the $M1$ contributions in ^{31}P , as shown in Fig. 1, and given in Table III. The $M1$ elastic cross sections were less than 5% of the experimental cross sections for all energies and angles.

IV. DATA ANALYSIS

Starting with a given charge distribution, $\rho(r)$, the differential cross sections for the elastic scattering of electrons were obtained by performing a numerical partial-wave analysis of the Dirac equation.^{7,8} The parameters of the charge distribution were varied until a best fit was obtained as indicated by the lowest χ^2 in the comparison of the measured differential cross sections and the calculated ones folded with the acceptance angle of the spectrometer. The correlated errors for the parameters were then calculated. Parameter errors arising from the $\pm 3\%$ uncertainty in the hydrogen calibration and the target-thickness uncertainties were found by refitting the data after shifting it to account for these systematic errors. These latter parameter errors were then added to the correlated parameter errors.

The experimental cross sections shown in Figs. 2 and 3 include all experimental corrections, and in Fig. 2 the $M1$ elastic scattering has been subtracted for ^{31}P . The data for ^{32}S are in good agreement with more extensive data of Li to be reported

TABLE I. Experimental results for ^{31}P . The differential cross sections and their errors are in the laboratory frame in units of millibarns per steradian.

Angle (deg)	Cross section (mb/sr)	Error (mb/sr)	Angle (deg)	Cross section (mb/sr)	Error (mb/sr)
^{31}P , 250.0 MeV			^{31}P , 250.0 MeV		
33.50	0.343	0.62×10^{-2}	89.50	0.175×10^{-4}	0.74×10^{-6}
35.50	0.219	0.31×10^{-2}	^{31}P , 400.0 MeV		
37.50	0.128	0.23×10^{-2}	33.50	0.198×10^{-2}	0.36×10^{-4}
39.50	0.778×10^{-1}	0.13×10^{-2}	35.50	0.511×10^{-3}	0.11×10^{-4}
41.50	0.446×10^{-1}	0.80×10^{-3}	37.50	0.238×10^{-3}	0.56×10^{-5}
43.50	0.262×10^{-1}	0.37×10^{-3}	39.50	0.273×10^{-3}	0.60×10^{-5}
45.50	0.144×10^{-1}	0.16×10^{-3}	41.50	0.290×10^{-3}	0.58×10^{-5}
47.50	0.797×10^{-2}	0.12×10^{-3}	43.50	0.271×10^{-3}	0.57×10^{-5}
49.50	0.404×10^{-2}	0.69×10^{-3}	45.50	0.238×10^{-3}	0.57×10^{-5}
51.50	0.188×10^{-2}	0.36×10^{-4}	47.50	0.172×10^{-3}	0.41×10^{-5}
53.50	0.867×10^{-3}	0.17×10^{-4}	49.50	0.128×10^{-3}	0.33×10^{-5}
55.50	0.393×10^{-3}	0.68×10^{-5}	51.50	0.795×10^{-4}	0.25×10^{-5}
57.50	0.167×10^{-3}	0.30×10^{-5}	53.50	0.459×10^{-4}	0.13×10^{-5}
59.50	0.971×10^{-4}	0.24×10^{-6}	55.50	0.229×10^{-4}	0.80×10^{-6}
61.50	0.827×10^{-4}	0.22×10^{-5}	57.50	0.133×10^{-4}	0.40×10^{-6}
63.50	0.864×10^{-4}	0.18×10^{-5}	59.50	0.556×10^{-5}	0.21×10^{-6}
65.50	0.970×10^{-4}	0.21×10^{-5}	61.50	0.235×10^{-5}	0.92×10^{-7}
67.50	0.103×10^{-3}	0.23×10^{-5}	63.50	0.797×10^{-6}	0.45×10^{-7}
69.50	0.113×10^{-3}	0.31×10^{-5}	65.50	0.236×10^{-6}	0.22×10^{-7}
71.50	0.998×10^{-4}	0.24×10^{-5}	69.50	0.179×10^{-6}	0.21×10^{-7}
73.50	0.857×10^{-4}	0.24×10^{-5}	72.50	0.227×10^{-6}	0.30×10^{-7}
75.50	0.773×10^{-4}	0.21×10^{-5}	75.50	0.238×10^{-6}	0.23×10^{-7}
77.50	0.659×10^{-4}	0.21×10^{-5}	78.50	0.199×10^{-6}	0.22×10^{-7}
79.50	0.534×10^{-4}	0.17×10^{-5}	80.50	0.157×10^{-6}	0.20×10^{-7}
81.50	0.446×10^{-4}	0.14×10^{-5}	83.50	0.80×10^{-7}	0.14×10^{-7}
83.50	0.348×10^{-4}	0.12×10^{-5}	86.50	0.40×10^{-7}	0.10×10^{-7}
85.50	0.279×10^{-4}	0.11×10^{-5}	89.50	0.22×10^{-7}	0.64×10^{-8}
87.50	0.208×10^{-4}	0.79×10^{-6}			

TABLE II. Experimental results for ^{32}S . The differential cross sections and their errors are in the laboratory frame in units of millibarns per steradian.

Angle (deg)	Cross section (mb/sr)	Error (mb/sr)	Angle (deg)	Cross section (mb/sr)	Error (mb/sr)
^{32}S , 250.0 MeV			^{32}S , 400.0 MeV		
33.50	0.366	0.55×10^{-2}	33.50	0.174×10^{-2}	0.30×10^{-4}
37.50	0.136	0.19×10^{-2}	35.50	0.515×10^{-3}	0.16×10^{-4}
41.50	0.455×10^{-1}	0.86×10^{-3}	39.50	0.315×10^{-3}	0.71×10^{-5}
45.50	0.138×10^{-1}	0.17×10^{-3}	43.50	0.293×10^{-3}	0.73×10^{-5}
49.50	0.377×10^{-2}	0.64×10^{-4}	47.50	0.164×10^{-3}	0.49×10^{-5}
53.50	0.798×10^{-3}	0.14×10^{-4}	51.50	0.622×10^{-4}	0.22×10^{-5}
57.50	0.171×10^{-3}	0.38×10^{-5}	55.50	0.175×10^{-4}	0.68×10^{-6}
61.50	0.103×10^{-3}	0.22×10^{-5}	59.50	0.316×10^{-5}	0.15×10^{-6}
65.50	0.121×10^{-3}	0.33×10^{-5}	63.50	0.296×10^{-6}	0.10×10^{-7}
69.50	0.111×10^{-3}	0.27×10^{-5}	67.50	0.216×10^{-6}	0.93×10^{-8}
73.50	0.911×10^{-4}	0.22×10^{-5}	72.50	0.339×10^{-6}	0.39×10^{-7}
77.50	0.602×10^{-4}	0.19×10^{-5}	78.50	0.205×10^{-6}	0.27×10^{-7}
81.50	0.386×10^{-4}	0.14×10^{-5}	83.50	0.64×10^{-7}	0.15×10^{-7}
85.50	0.233×10^{-4}	0.91×10^{-6}			
89.50	0.122×10^{-4}	0.59×10^{-6}			

in a separate publication.¹¹ The errors shown include target-thickness uncertainties, other experimental errors, and statistical errors. For the 250-MeV data and for forward-angle data the errors are smaller than the experimental points shown in the figure. The elastic scattering data analysis was carried out with a numerical partial-wave computer code⁷ revised for use on the CDC-3600/3800 computer at the University of Massachusetts.⁸

The 250-MeV data and most of the 400-MeV ³¹P data were fitted by using the parabolic Fermi charge distribution

$$\rho(r) = \rho_0(1 + wr^2/c^2)(1 + e^{(r-c)/z})^{-1}, \quad (1)$$

where ρ_0 is a normalization constant, and c , z , and w are three adjustable parameters. The last few higher-momentum-transfer large-angle points for ³¹P required the addition to Eq. (1) of a modulation $\Delta\rho(r)$ so that $\rho(r)$ took a form similar to the one described by Bellicard *et al.*,²

$$\rho(r) = \rho_0 \left[\frac{1 + w(r/c)^2}{1 + e^{(r-c)/z}} + A' \frac{\sin q_0 r}{q_0 r} e^{p_0^2 r^2/4} \right], \quad (2)$$

where A' , p_0 , and q_0 are additional adjustable parameters. This charge distribution was used in

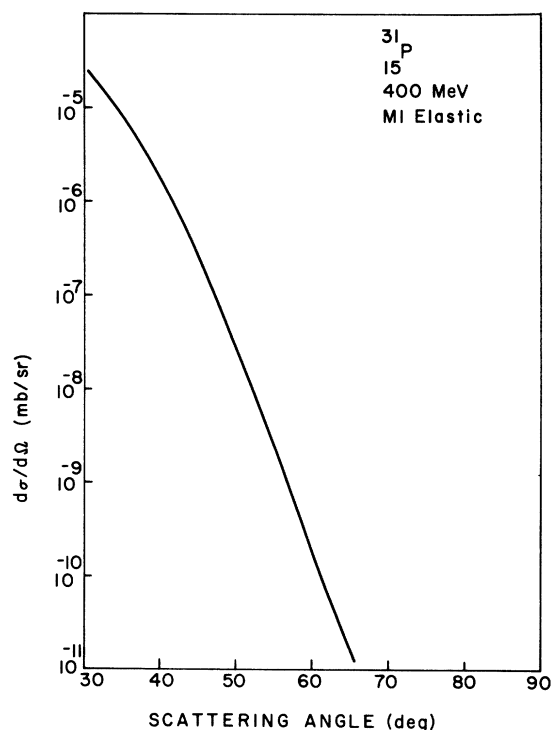


FIG. 1. Cross sections calculated for the elastic scattering of 400.0-MeV electrons from the magnetic dipole moment of ³¹P versus scattering angle.

the phase-shift calculation for obtaining simultaneous fits to all experimental cross sections for all q 's. The complete set of best-fit parameters together with the rms charge radius, $\langle r^2 \rangle^{1/2}$, are given in Table IV. The best-fit calculated cross section curves are shown in Figs. 2 and 3, and the corresponding charge distributions for ³¹P are shown in Fig. 4.

V. DISCUSSION

For ³¹P there is only one other published elastic electron scattering result with which to compare these results: the low-momentum-transfer work of Kossanyi-Demay, Lombard, and Bishop.¹² They obtained a fit to their data with a two-parameter Fermi distribution with values of $c = 3.21$ fm and $z = 0.56$ fm. The corresponding rms radius is 3.07 fm. Elton and Swift¹³ have used central Woods-Saxon single-particle potentials for the $1p$ and $2s-1d$ shells to fit the data of Kossanyi-Demay, Lombard, and Bishop.¹² They obtain an rms radius of 3.24 fm. For the higher-momentum-transfer ³¹P data of this experiment, which required additional fitting parameters, as given in Eq. (2), we obtained an rms charge radius of 3.19 ± 0.03

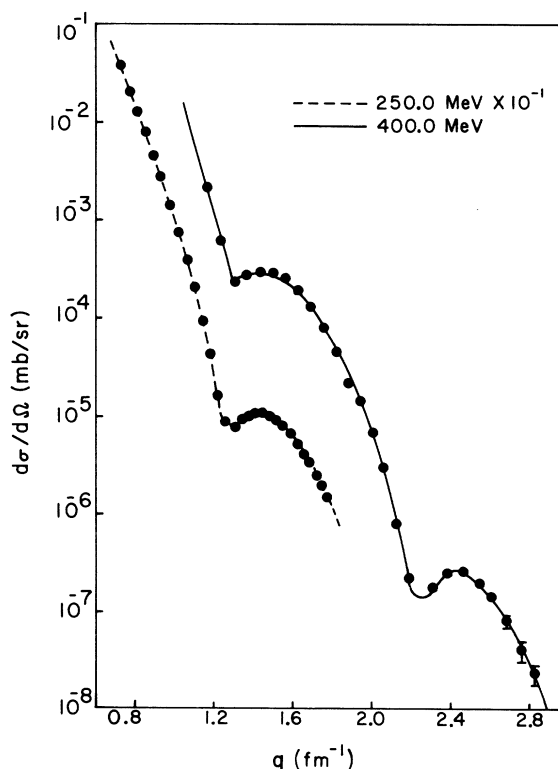


FIG. 2. Experimental cross sections for the elastic scattering from ³¹P of 250.0- and 400.0-MeV electrons versus momentum transfer.

fm. This value agrees with the value 3.188 ± 0.018 fm obtained by Wu and Willets¹⁴ from muonic x-ray analysis. The ^{32}S parameters of Li, Sick, and Yearian,¹¹ who have taken more extensive and higher momentum transfer data than in this experiment, give an excellent fit to the data of Table II. The rms charge radius for ^{32}S obtained in this experiment and by Li, Sick, and Yearian, 3.245 ± 0.032 fm, is in excellent agreement with the muonic x-ray value¹⁴ of 3.244 ± 0.018 fm.

Also shown in Fig. 4 is the charge density of ^{31}P calculated¹⁵ by using Woods-Saxon potentials whose parameters given in Table V were separately adjusted for s and d states and for p states to fit the rms radii, and the known separation energies. Also a 0.8-fm mean-radius Gaussian proton distribution was folded into the distribution of proton centers. There is good agreement between the experimental phenomenological charge distribution and the shell-model result for the case of ^{31}P , but there is poor agreement near the origin for the case of ^{32}S . The $\Delta\rho$ as given by Eq. (2) is negative at the origin in the case of ^{31}P , whereas it is positive at the origin for 500-MeV ^{32}S data obtained by Li, Sick, and Yearian.¹¹

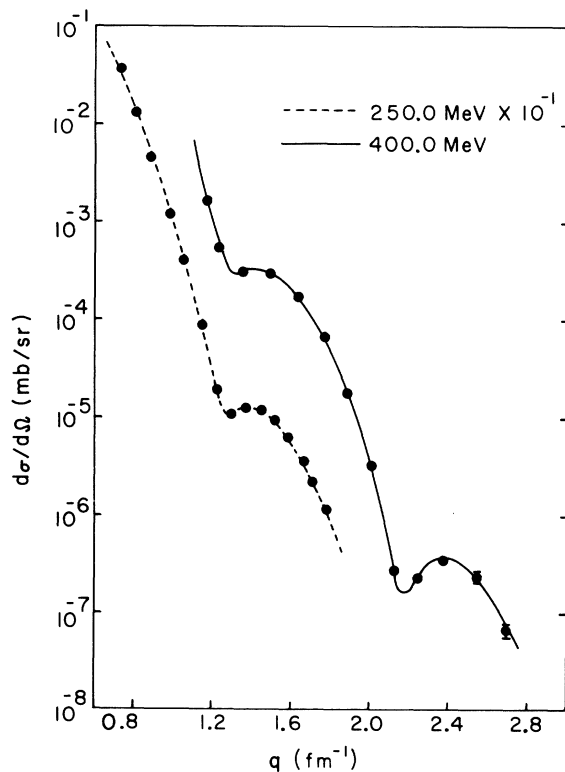


FIG. 3. Experimental cross sections for the elastic scattering from ^{32}S of 250.0- and 400.0-MeV electrons versus momentum transfer.

In Fig. 5 is shown the difference between the ^{32}S and the ^{31}P phenomenological charge distributions multiplied by $4\pi r^2$, a quantity better determined by electron scattering experiments than the charge-density difference itself. This weighting of the charge-density difference by $4\pi r^2$ reduces the importance of the region near the origin, a region which has been shown¹⁶ to be somewhat dependent upon the phenomenological model used in fitting electron scattering data. There is a prominent peak at about 4.0 fm and an indication of a peak at about 1.2 fm. Such a two-peak structure is characteristic of a $2s_{1/2}$ harmonic-oscillator wave function as shown in Fig. 6. The difference in the shell-model charge distributions also shows the pronounced two-peak behavior.

The error bars shown in Figs. 5 and 6 are based entirely upon the errors in the parameters c , z , and w as determined by finding a variation of unity in the χ^2 surface representing the fits to the data using these parameters. The parameters c , z , and w were allowed to take on all combinations to the full ranges of their uncertainties as calculated in the χ^2 analysis, consistent with the rms radius not exceeding its uncertainty, as well as allowing

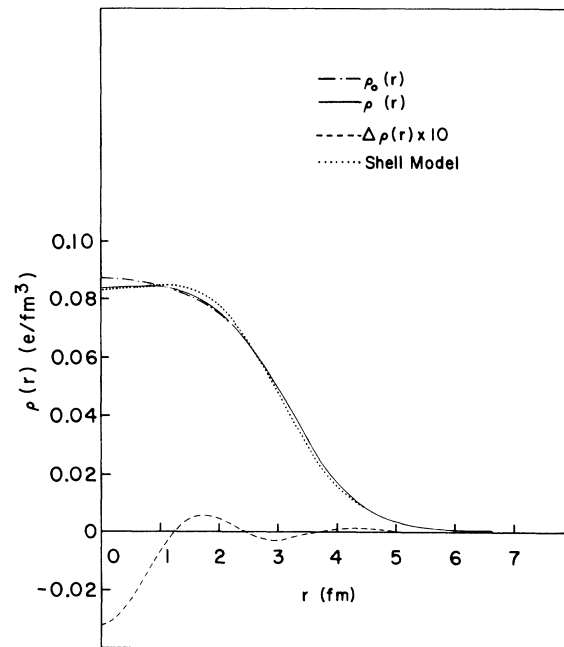


FIG. 4. The charge distribution of ^{31}P . The dashed-dot curve labeled $\rho_0(r)$ is the three-parameter distribution of Eq. (1). The solid curve is the six-parameter distribution of Eq. (2) with the best-fit parameters obtained by simultaneously fitting all of the data of Fig. 2. The lower dashed curve is twice the oscillatory second term of Eq. (2). The dotted curve labeled "shell model" is the result of a calculation using Woods-Saxon well parameters as given in Table V.

TABLE III. Calculated $M1$ elastic contributions for ^{31}P in percent of the experimental cross sections of Table I.

250 MeV		400 MeV	
θ (deg)	$(d\sigma/d\Omega)_{M1}$ (%)	θ (deg)	$(d\sigma/d\Omega)_{M1}$ (%)
33.50	0.01	33.50	0.60
39.50	0.03	37.50	1.70
45.50	0.13	39.50	0.73
51.50	0.63	41.50	0.34
55.50	2.05	45.50	0.08
61.50	4.57	47.50	0.05
65.50	2.34	49.50	0.03
69.50	1.14	53.50	0.01
73.50	0.84	57.50	0.006
77.50	0.64	59.50	0.005
81.50	0.53	63.50	0.003
89.50	0.48	69.50	0.001
		75.50	0.000

for the 2% target-thickness errors. The 3% uncertainty in the usual hydrogen normalization does not enter for the data which were obtained at the same time for the two nuclei. In this manner the errors in the two charge densities were found and then added together for the difference curves. The resulting errors are shown centered around the difference of the three-parameter distributions. The values of c , z , and w used in the three-parameter distributions are the same as those of Table IV. It can be seen that there is little difference between the six-parameter charge-density-difference curve and the three-parameter one. The shape of the difference curve is determined primarily by the low- q data.

It can be seen from Fig. 6 that both the harmonic-oscillator and the Woods-Saxon models do not completely account for the charge-density differences, although they do give agreement for most

TABLE IV. Charge-distribution best-fit parameters. Numerical values for ^{31}P and ^{32}S of the best-fit parameters of the parabolic Fermi charge distribution with an additional oscillatory term [Eq. (2)].

	^{31}P	$^{32}\text{S}^a$
c (fm)	3.369 ± 0.025	3.441 ± 0.024
z (fm)	0.582 ± 0.006	0.624 ± 0.006
w	-0.173 ± 0.024	-0.213 ± 0.014
q_0 (fm $^{-1}$)	2.48 ± 0.07	3.41 ± 0.04
p_0 (fm $^{-1}$)	0.51 ± 0.11	0.37 ± 0.05
A'	-0.034 ± 0.008	0.036 ± 0.004
$\langle r^2 \rangle^{1/2}$ (fm)	3.19 ± 0.03	3.245 ± 0.032

^a The ^{32}S charge-distribution parameters are those of Li, Sick, and Yearian (Ref. 11).

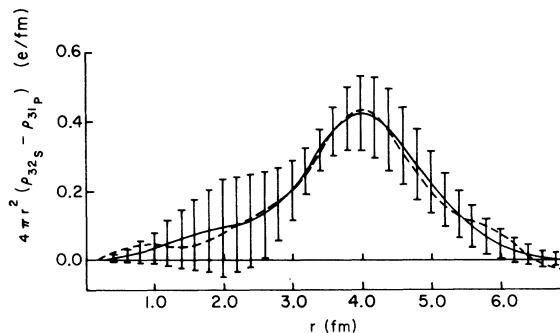


FIG. 5. The difference between the phenomenological best-fit charge distributions of ^{32}S and ^{31}P multiplied by $4\pi r^2$ for the three-parameter distributions of Eq. (1) (solid curve) and for the six-parameter distributions of Eq. (2) (dashed curve). The error bars are based entirely upon the errors in c , z , and w .

of the radial range within the rather large errors. This indicates that the $2s_{1/2}$ proton retained its identity in some respects in the ^{32}S nucleus. The role of nuclear rearrangement caused by the changes in the nuclear field due to the addition of the $2s_{1/2}$ proton, as well as configuration mixing, need investigation, and may be the cause of the disagreement.

The method of data analysis of this experiment involving simultaneous fitting of the data ignored possible energy-dependent effects, such as virtual nuclear excitations,¹⁷ wherein a nucleus is raised to an excited state by the absorption of a virtual photon while making a transition to the ground state via a second-exchanged virtual photon. Since conclusive experimental information on such effects does not exist at this time, we assumed a static charge distribution as our model, as is the usual approach in this type of analysis.

TABLE V. Woods-Saxon potential well parameters used in obtaining shell-model charge distributions.

	Depth (MeV)			
	V_0 Central	V_{so} (spin-orbit)	a (fm)	r_0 (fm)
^{31}P				
p states	68.8	21.0	0.65	1.275
s and d states ($\langle r^2 \rangle^{1/2} = 3.19$ fm)	53.9	17.0	0.65	1.275
^{32}S				
p states	65.1	14.0	0.65	1.28
s and d states ($\langle r^2 \rangle^{1/2} = 3.245$ fm)	56.8	18.0	0.65	1.28

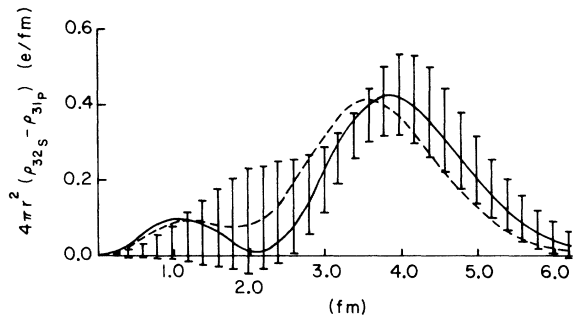


FIG. 6. The difference between the shell-model charge distributions of ^{32}S and ^{31}P multiplied by $4\pi r^2$ which were calculated by using the harmonic-oscillator approximation (solid curve) and by using the Woods-Saxon well parameters of Table V (dashed curve). The error bars are those of Fig. 5.

ACKNOWLEDGMENTS

We wish to thank Professor W. Gerace for his help and advice pertaining to this work. Two of us (B.B.P.S. and G.A.P.) wish to thank Professor Hofstadter and Professor Yearian and their staff for the opportunity to perform this experiment at Stanford.

†Part of this work was submitted by B. B. P. Sinha to the faculty of the University of Massachusetts in partial fulfillment of the requirement for the degree of Doctor of Philosophy.

*Work supported in part by the National Science Foundation under Grant No. NSF GP-28611, the Office of Naval Research under Contract No. NONR 225(67), and by grants from the Research Council of the University of Massachusetts.

‡Present address: Department of Physics, University of Toronto, Toronto 5, Canada.

§Present address: Department of Physics, University of Massachusetts, Amherst, Massachusetts 01002.

¹R. F. Frosch, R. Hofstadter, J. S. McCarthy, G. K. Nöldeke, K. J. van Oostrum, M. R. Yearian, B. C. Clark, R. Herman, and D. G. Ravenhall, *Phys. Rev.* **174**, 1380 (1968).

²J. B. Bellicard, P. Bounin, R. F. Frosch, R. Hofstadter, J. S. McCarthy, B. C. Clark, R. Herman, and D. G. Ravenhall, *Phys. Rev. Letters* **19**, 527 (1967).

³B. B. P. Sinha, G. A. Peterson, R. R. Whitney, I. Sick, and J. S. McCarthy, to be published.

⁴B. B. P. Sinha, G. A. Peterson, I. Sick, and J. S. McCarthy, *Phys. Letters* **35B**, 217 (1971).

⁵L. R. Suelzle and M. R. Yearian, in *Proceedings of the International Conference on Nucleon Structure*, edited by R. Hofstadter and L. I. Schiff (Stanford U. P.,

The major experimental errors could be reduced substantially in future studies by better determination of target thicknesses, and by taking precise relative low- q measurements in order to determine more accurate rms radii. Also separate measurements of magnetic contributions by 180° scattering would reduce this uncertainty for the odd- A isotones.

Future high-resolution equipment capable of separating low-lying inelastic peaks from the elastic peak may permit the study of longer chains of isotones in analogy with isotopes. Properly interpreted precise studies of isotones, together with isotopes, should provide a new source of information about single particle radial wave functions.

Stanford, California, 1964), p. 360.

⁶P. J. Friedl, C. Sederholm W. Dye, H. Crannell, and M. R. Yearian, *J. Computational Phys.* **1**, 305 (1967).

⁷J. Heisenberg, private communication; D. R. Yennie, D. G. Ravenhall, and R. N. Wilson, *Phys. Rev.* **95**, 500 (1954).

⁸B. B. P. Sinha, Ph.D. thesis, University of Massachusetts at Amherst, 1971 (unpublished).

⁹T. A. Griffy and D. U. Yu, *Phys. Rev.* **139**, B880 (1965).

¹⁰T. DeForest, Jr., and J. D. Walecka, *Advan. Phys.* **15**, 1 (1966).

¹¹G. C. Li, I. Sick, and M. R. Yearian, *Phys. Letters* **37B**, 282 (1971). A complete report of this work will appear in a later publication.

¹²P. Kossanyi-Demay, R. Lombard, and G. R. Bishop, *Nucl. Phys.* **62**, 615 (1965).

¹³L. R. B. Elton and A. Swift, *Nucl. Phys.* **A94**, 52 (1967).

¹⁴C. S. Wu and L. Willets, *Ann. Rev. Nucl. Sci.* **19**, 527 (1969).

¹⁵W. J. Gerace and G. C. Hamilton, *Phys. Letters* **39B**, 481 (1972).

¹⁶J. Friedrich and F. Lenz, *Nucl. Phys.* **183**, 523 (1972).

¹⁷P. Unginçius, H. Überall, and G. H. Rawitscher, *Nucl. Phys.* **A158**, 418 (1970).